IEMS Vol. 9, No. 4, pp. 323-338, December 2010.

Modeling Implied Volatility Surfaces Using Two-dimensional Cubic Spline with Estimated Grid Points

Seung-Ho Yang
Department of Industrial and Management Engineering
Pohang University of Science and Technology, Pohang, Kyungbuk, 790-784, KOREA
Tel: +82-54-279-8258, E-mail: grimaysh@postech.ac.kr

Jaewook Lee
Department of Industrial and Management Engineering
Pohang University of Science and Technology, Pohang, Kyungbuk, 790-784, KOREA
Tel: +82-54-279-2209, E-mail: jaewookl@postech.ac.kr

Gyu-Sik Han†
Division of Business Administration
Chonbuk National University, 1- Ga Deokjin-dong, Jeon-ju, Chonbuk, 561-756, KOREA
Tel: +82-63-270-2984, E-mail: gshan0815@jbnu.ac.kr

Received, February 27, 2010; Revised, May 20, 2010; Accepted, May 20, 2010

Abstract. In this paper, we introduce the implied volatility from Black-Scholes model and suggest a model for constructing implied volatility surfaces by using the two-dimensional cubic (bi-cubic) spline. In order to utilize a spline method, we acquire grid (knot) points. To this end, we first extract implied volatility curves weighted by trading contracts from market option data and calculate grid points from the extracted curves. At this time, we consider several conditions to avoid arbitrage opportunity. Then, we establish an implied volatility surface, making use of the two-dimensional cubic spline method with previously estimated grid points. The method is shown to satisfy several properties of the implied volatility surface (smile, skew, and flattening) as well as avoid the arbitrage opportunity caused by simple match with market data. To show the merits of our proposed method, we conduct simulations on market data of S&P500 index European options with reasonable and acceptable results.

Keywords: Implied Volatility Surface, Arbitrage, Two-dimensional Cubic Spline, S&P500 Index European option

1. INTRODUCTION

The option pricing formula of the Black-Scholes model is still the most widely used amongst market practitioners (Han and Lee, 2008; Han *et al*., 2009). The main merits of the model include their simplicity, robustness, and ease of implementation. The only unknown parameter in the pricing formula is the volatility of the underlying. In order to obtain it, the historical volatility was proposed and several methods to calculate it has been developed (Parkinson, 1980; Rogers and Satchell, 1991; Rogers *et al*., 1994). The option prices using the historical volatility mismatch with the real market option prices since the assumptions of the Black-Scholes model do not satisfy the real market properties. Therefore, instead of the historical volatility, the implied volatility surface (IVS) attained from inverting the Black-Scholes formula is used for consistent valuation of the derivatives with the financial markets (Black and Scholes, 1973). In other words, the IVS is used for the absence of arbitrage. We usually build the IVS according to the forward-moneyness, which is the strike price divided by the forward price of an underlying asset, and time to expiry. In general, IVS has the shape of smile with the moneyness and the level of im-

† : Corresponding Author

plied volatilities increases or decreases according to the level of the time to maturity. Since the option prices evaluated by Black-Scholes formula are equal to the real market option prices with implied volatility, modeling the IVS directly becomes a major concern recently. There are several methods to formulate the implied volatility surface (Cont and da Fonseca, 2002; Dumas *et al*., 1998; Konstantinidi *et al*., 2008). Especially, local volatility models that were originally studied by Dupire, Derman *et al*., and Rubinstein and inserted into highly efficient pricing models by Andersen *et al*. and Dempster *et al*. are very much dependent on an estimate of the IVS (Andersen and Brotherton-Ratcliffe, 1997; Dempster and Richards, 2000; Derman and Kani, 1994; Dupire, 1994; Fengler, 2005; Kim *et al*., 2009; Rubinstein, 1994). The estimate should be free of arbitrage. Otherwise, negative transition probabilities or negative volatilities might be produced, which can make the algorithm solving the generalized Black-Scholes partial differential equation not to converge.

In this paper, we propose a method that builds the IVS, using two-dimensional cubic spline to satisfy several arbitrage-free conditions. The proposed method consists of two phases: the first phase for optimizing a constrained objective function to look for the implied volatilities to be used as the grid points of the two-dimensional cubic spline and the second phase for constructing the IVS with use of the grid points we find in the first phase. The proposed method will, through simulation results, be shown to fit well the real market implied volatility values. The paper is structured as follows. In Section 2, we give some preliminary notions and terminologies that are needed for the subsequent sections. In Section 3, we provide detailed explanations to generate an objective function with arbitrage-free constraints and to construct an IVS with two-dimensional cubic spline. Then we show the simulation results in Section 4 and conclude this paper in Section 5.

2. PRELIMINARY

2.1 Black-Scholes Option Pricing Formula

Black-Scholes model is a major breakthrough for pricing options in the financial engineering. It is one of the most well-known and widely used methods. There are several assumptions to derive this formula as follows:

1. The underlying asset price in the model follows a geometric Brownian motion with constant drift, volatility, and interest rate is fixed.
2. The model assumes no transaction costs and taxes, and all securities can be perfectly divisible.

In the case of paying continuous yield dividends the Black-Scholes formula for the European call and put option prices, denoted by V_{Call} and V_{Put}, are given by

$$C_{BS}(S_0, K, \tau, \Sigma, r, \delta) = e^{-r\tau}\{F_0 N(d_1) - KN(d_2)\} \quad (1)$$

$$P_{BS}(S_0, K, \tau, \Sigma, r, \delta) = e^{-r\tau}\{KN(-d_2) - F_0 N(-d_1)\} \quad (2)$$

$$d_1 = \frac{\ln(F_0/K) + 0.5\Sigma^2\tau}{\Sigma\sqrt{\tau}}, \quad d_2 = d_1 - \Sigma\sqrt{\tau}$$

where S_0 is the present underlying price, K is the strike price, τ is the time to expiry date, Σ is the volatility of the underlying, N is the cumulative function of a standard normal distribution, r is the risk-free interest rate, δ is the continuous dividend rate, and F_0 is the forward price of the underlying. The forward price is calculated as follow:

$$F_0 = S_0 e^{(r-\delta)\tau}$$

2.2 Implied Volatility

The volatility is used in the Black-Scholes formula, but the financial market does not provide it explicitly. Though it could be obtained by means of time-series underlying asset prices, the option price generated by the realized volatility of past market data would not match with the market option prices. That stems from the fact that the assumptions of the Black-Scholes formula are too simple to apply to the real market. Hence the implied volatility, which equated the calculated price to the real market price, is one of choices. Implied volatility can be represented in terms of the Black-Scholes formula:

$$C_{BS}(S_0, K, \tau, \Sigma_{im}(K/F_0, \tau), r, \delta) = C_{market}$$
$$P_{BS}(S_0, K, \tau, \Sigma_{im}(K/F_0, \tau), r, \delta) = P_{market}$$

where C_{market} and P_{market} denote the observed market European call price and put price, respectively, and $\Sigma_{im}(K/F_0,\tau)$ is the implied volatility depending on $(K/F_0, \tau)$. Here K/F_0 is called forward-moneyness.

3. RESEARCH METHODOLOGY

In this section, we provide a way to construct an IVS, using two-dimensional cubic spline based on the implied volatilities of the two-dimensional grid points that are computed through optimization. Although we can use local quadratic polynomial to establish the implied volatility surface directly, it has some drawbacks. It's hard to choose the optimal bandwidth of the kernel function in two-dimensional case and which kernel performs well (Kim *et al*., 2009). The proposed method basically consists of two parts. To begin with, we calculate the implied volatilities of grid points through optimization, having no-arbitrage and calendar-spread-free conditions. Then, we construct the IVS with two-dimensional cubic spline using the implied volatilities of the grid points.

3.1 Calculating Implied Volatility of Grid Points with constraints free of arbitrage

To compute the implied volatilities of the grid points,

we first establish following model to fit the real market implied volatilities in each time to maturities.

$$\Sigma^2(k,\tau) = a_0 + a_1(k - a_2)^2 \tag{3}$$

where

$$a_0 \geq 0,\ a_1 \geq 0,\ k = \ln(K/F_0)$$

We usually call k and τ *log forward-moneyness* and *time to maturity*, respectively. Since the implied volatility cannot have negative value, we add some constraints on a_0 and a_1. In the case of equity options, the implied volatility shows closely linear change as the forward-money-ness goes higher (i.e. deep-out-of-the-money put or deep-in-the-money call) while it increases abruptly as the moneyness decreases from one, which means the at-the-money option (Hull, 2009). Thus, we set the variance function as the perfect square function. Based on this model we can calculate risk-neutral probability density function.

Proposition: *The cumulative risk-neutral probability density function* (Φ) *based on the implied volatility model, Eq. (3), is*

$$\Phi(k,\tau\,|F_0) = 1 - N(d_2) + F_0\dot{d}_1 n(d_1) - K\dot{d}_2 n(d_2)$$

where

$$N(x) = \int_{-\infty}^{x} n(y)dy,\ n(y) = \frac{1}{\sqrt{2\pi}}e^{-y^2/2}$$

$$\dot{d}_1 = \frac{\partial d_1}{\partial K} = -\frac{1}{K\Sigma\sqrt{\tau}} - \frac{1}{\Sigma^2\sqrt{\tau}}\ln\left(\frac{F_0}{K}\right)\dot{\Sigma} + \frac{1}{2}\dot{\Sigma}\sqrt{\tau}$$

$$\dot{d}_2 = \frac{\partial d_2}{\partial K} = -\frac{1}{K\Sigma\sqrt{\tau}} - \frac{1}{\Sigma^2\sqrt{\tau}}\ln\left(\frac{F_0}{K}\right)\dot{\Sigma} - \frac{1}{2}\dot{\Sigma}\sqrt{\tau}$$

$$\dot{\Sigma} = \frac{\partial \Sigma}{\partial K} = \frac{1}{K}\Sigma^{-1}a_1\left\{\ln\left(\frac{F_0}{K}\right) - a_2\right\}$$

Then the risk-neutral probability function (φ) is as follows:

$$\varphi(k,\tau\,|F_0) = \frac{\partial \Phi}{\partial K} = -2\dot{d}_2 n(d_2) + F_0\ddot{d}_1 n(d_1) + F_0(\dot{d}_1)^2\dot{n}(d_1) - K\ddot{d}_2 n(d_2) - K(\dot{d}_2)^2\dot{n}(d_2)$$

where

$$\ddot{d}_1 = \frac{\partial^2 d_1}{\partial K^2} = \frac{1}{K^2\Sigma\sqrt{\tau}} + \frac{1}{K\Sigma^2\sqrt{\tau}}\dot{\Sigma} + \frac{2}{\Sigma^3\sqrt{\tau}}\ln\left(\frac{F_0}{K}\right)\dot{\Sigma} + \frac{1}{K\Sigma^2\sqrt{\tau}}\dot{\Sigma} - \frac{1}{\Sigma^2\sqrt{\tau}}\ln\left(\frac{F_0}{K}\right)\ddot{\Sigma} + \frac{1}{2}\ddot{\Sigma}\sqrt{\tau}$$

$$\ddot{d}_2 = \frac{\partial^2 d_2}{\partial K^2} = \frac{1}{K^2\Sigma\sqrt{\tau}} + \frac{1}{K\Sigma^2\sqrt{\tau}}\dot{\Sigma} + \frac{2}{\Sigma^3\sqrt{\tau}}\ln\left(\frac{F_0}{K}\right)\dot{\Sigma} + \frac{1}{K\Sigma^2\sqrt{\tau}}\dot{\Sigma} - \frac{1}{\Sigma^2\sqrt{\tau}}\ln\left(\frac{F_0}{K}\right)\ddot{\Sigma} - \frac{1}{2}\ddot{\Sigma}\sqrt{\tau}$$

$$\dot{n}(d_1) = -\dot{d}_1 d_1 \frac{1}{\sqrt{2\pi}}e^{-(d_1)^2/2}$$

$$\dot{n}(d_2) = -\dot{d}_2 d_2 \frac{1}{\sqrt{2\pi}}e^{-(d_2)^2/2}$$

$$\ddot{\Sigma} = \frac{\partial^2 \Sigma}{\partial K^2} = -\frac{1}{K^2}\Sigma^{-1}a_1\left\{\ln\left(\frac{F_0}{K}\right) - a_2\right\} - \frac{1}{K}\Sigma^{-2}\dot{\Sigma}a_1\left\{\ln\left(\frac{F_0}{K}\right) - a_2\right\} + \frac{1}{K^2}\Sigma^{-1}a_1 \qquad \square$$

The detailed proof of the proposition is explained in Appendix. For each τ_j we calibrate parameters a_0, a_1, and a_2 through following objective function under no-arbitrage conditions (Breeden and Litzenberger, 1978; Carr and Madan, 2005; Fengler, 2005):

$$\arg\min_{\theta_j} \sum_{i=1}^{n} w_i \left|\Sigma_j^{\text{model}}(k_i,\tau_j) - \Sigma_j^{\text{market}}(k_i,\tau_j)\right|^2 \tag{4}$$

$$\text{where } \theta_j = \{a_0^j, a_1^j, a_2^j\}$$

subject to

$$a_0^j,\ a_1^j \geq 0 \tag{5}$$

$$-e^{r\tau_j} \leq \frac{\partial C_{BS}(k_i,\tau_j,\Sigma_j^{\text{model}}(k_i,\tau_j),r,\delta\,|F_0)}{\partial K} \leq 0 \tag{6}$$

$$\varphi(k_i,\tau_j,\Sigma_j^{\text{model}}(k_i,\tau_j)\,|F_0) \geq 0 \tag{7}$$

$$\max(F_0 - K, 0) \leq e^{r\tau_j}C_{BS}(k_i,\tau_j,\Sigma_j^{\text{model}}(k_i,\tau_j),r,\delta\,|F_0) \leq F_0 \tag{8}$$

In Eq. (4), Σ_j^{market} is the observed implied volatilities for the moneyness k_i and time to maturity τ_j, Σ_j^{model} is the implied volatility computed by the perfect square function defined in Eq. (3), and w_i is the weight of the difference between Σ_i^{market} and Σ_i^{model}. It is computed as the logarithm of the number of trading contracts for the ith option added to 1. After calibrating parameters a_0^j, a_1^j, and a_2^j for τ_j, we include one more condition of the calendar spread for τ_{j+1} in the following way (Carr and Madan, 2005), optimizing the three parameters, a_0^{j+1}, a_1^{j+1}, and a_2^{j+1}, with their initial values as a_0^j, a_1^j, and a_2^j:

$$\forall i = 1,2,\cdots,n\ \ C_{BS}(k_i,\tau_j,\Sigma_j^{\text{model}}(k_i,\tau_j),r,\delta\,|F_0) \leq C_{BS}(k_i,\tau_{j+1},\Sigma_{j+1}^{\text{model}}(k_i,\tau_{j+1}),r,\delta\,|F_0),\ \text{if } \tau_{j+1} \geq \tau_j \tag{9}$$

Through the optimization procedure referred above, we use the *interior-point algorithm* that is based on conjugate gradient calculations. The optimization method is explained in Appendix.

3.2 Building Implied Volatility Surface with Two-dimensional Cubic Spline

In order to calculate the implied volatilities of the grid points, we establish the grid points of the forward-

moneyness values, k_i, and the time to maturities, τ_j. We choose the moneyness points, which are equally divided in some region, and set the time to maturities as the time to maturities of the real market data. We establish the grid points of the moneyness value and time to expiry in the following way:

$$\gamma = \tau_1 < \tau_2 < \cdots < \tau_m = \eta \ \ (m \geq 2) \tag{10}$$

$$\alpha = k_1 < k_2 < \cdots < k_m = \beta \ \ (m \geq 2) \tag{11}$$

Then, we can calculate the implied volatilities of the grid points in each time to maturity from the parameter set, θ_j, calibrated in Eq. (4). Using the implied volatilities of the grid points, we can model the implied volatility surface using the two-dimensional cubic spline. The input vector X can be represented by

$$X_{ij} = (k_i, \tau_j), \ \ i = 1, 2, \cdots, n \ \ \text{and} \ \ \ j = 1, 2, \cdots, m$$

This rectangle is subdivided into (n-1)(m-1) subrectangles, R_{ij}:

$$R_{ij} = \left\{ (k, \tau) \,\middle|\, k_i < k < k_{i+1}, \tau_j < \tau < \tau_{j+1} \right\}$$

Then the implied volatilities, Σ_{ij}, can be modeled using the two-dimensional cubic spline function as follows:

$$\Sigma_{ij}(k, \tau) = \sum_{p=1}^{4} \sum_{q=1}^{4} c_{ijpq} (k - k_i)^{p-1} (\tau - \tau_j)^{q-1} \tag{12}$$

$$(k, \tau) \in R_{ij}, \ i = 1, 2, \cdots, n-1 \ \ \text{and} \ \ j = 1, 2, \cdots, m-1$$

We calculate the coefficients of the two-dimensional cubic spline function utilizing the implied volatilities of the grid points. The method is presented by de Boor (de Boor, 1962). It consists of several steps. At first, we consider the third-order bi-cubic function that has the subrectangle R on the interpolation nodes as grid points:

$$\Sigma_{ij}(k, \tau) = \begin{pmatrix} g_{i1}(k) & g_{i2}(k) & g_{i3}(k) & g_{i4}(k) \end{pmatrix} C \begin{pmatrix} g_{j1}(\tau) \\ g_{j2}(\tau) \\ g_{j3}(\tau) \\ g_{j4}(\tau) \end{pmatrix} \tag{13}$$

where $g_{ip}(k) = (k-k_i)^{p-1}$, $g_{jq}(\tau) = (\tau-\tau_j)^{q-1}$, and the coefficient matrix C is the following 4-by-4 matrix:

$$C = \begin{pmatrix} c_{ij11} & c_{ij12} & c_{ij13} & c_{ij14} \\ c_{ij21} & c_{ij22} & c_{ij23} & c_{ij24} \\ c_{ij31} & c_{ij32} & c_{ij33} & c_{ij34} \\ c_{ij41} & c_{ij42} & c_{ij43} & c_{ij44} \end{pmatrix} \tag{14}$$

Next, we determine the 16(n-1)(m-1) coefficients in Eq. (14). We can use the property that the implied volatility function ($\sum_{ij}$) satisfies the C^2 requirements in the k and τ directions yield. To determine the mixed partial derivative at each node, we introduce the connection matrix J satisfying the below condition:

$$J = V(k_i) C \left[V(\tau_j) \right]^T$$

with

$$J = \begin{pmatrix} u_{ij} & q_{ij} & u_{i,j+1} & q_{i,j+1} \\ p_{ij} & r_{ij} & p_{i,j+1} & r_{i,j+1} \\ u_{i+1,j} & q_{i+1,j} & u_{i+1,j+1} & q_{i+1,j+1} \\ p_{i+1,j} & r_{i+1,j} & p_{i+1,j+1} & r_{i+1,j+1} \end{pmatrix} \tag{15}$$

In Eq. (15), each element is computed by Späth (Späth, 1995) and referred in Appendix. Then, we can make the connection matrix as follows:

$$\Delta k_i = k_{i+1} - k_i, \ \ \Delta \tau_j = \tau_{j+1} - \tau_j$$

$$V(k_i) = \begin{pmatrix} g_{i1}(k_i) & g_{i2}(k_i) & g_{i3}(k_i) & g_{i4}(k_i) \\ \dot{g}_{i1}(k_i) & \dot{g}_{i2}(k_i) & \dot{g}_{i3}(k_i) & \dot{g}_{i4}(k_i) \\ g_{i1}(k_{i+1}) & g_{i2}(k_{i+1}) & g_{i3}(k_{i+1}) & g_{i4}(k_{i+1}) \\ \dot{g}_{i1}(k_{i+1}) & \dot{g}_{i2}(k_{i+1}) & \dot{g}_{i3}(k_{i+1}) & \dot{g}_{i4}(k_{i+1}) \end{pmatrix} = \begin{pmatrix} 1 & 0 & 0 & 0 \\ 0 & 1 & 0 & 0 \\ 1 & \Delta k_i & (\Delta k_i)^2 & (\Delta k_i)^3 \\ 0 & 1 & 2\Delta k_i & 3(\Delta k_i)^2 \end{pmatrix}$$

$$V(\tau_j) = \begin{pmatrix} g_{j1}(\tau_j) & g_{j2}(\tau_j) & g_{j3}(\tau_j) & g_{j4}(\tau_j) \\ \dot{g}_{j1}(\tau_j) & \dot{g}_{j2}(\tau_j) & \dot{g}_{j3}(\tau_j) & \dot{g}_{j4}(\tau_j) \\ g_{j1}(\tau_{j+1}) & g_{j2}(\tau_{j+1}) & g_{j3}(\tau_{j+1}) & g_{j4}(\tau_{j+1}) \\ \dot{g}_{j1}(\tau_{j+1}) & \dot{g}_{j2}(\tau_{j+1}) & \dot{g}_{j3}(\tau_{j+1}) & \dot{g}_{j4}(\tau_{j+1}) \end{pmatrix} = \begin{pmatrix} 1 & 0 & 0 & 0 \\ 0 & 1 & 0 & 0 \\ 1 & \Delta \tau_j & (\Delta \tau_j)^2 & (\Delta \tau_j)^3 \\ 0 & 1 & 2\Delta \tau_j & 3(\Delta \tau_j)^2 \end{pmatrix}$$

The inverse matrices of $V(k_i)$ and $V(\tau_j)$ can be calculated as

$$\left[V(k_i) \right]^{-1} = \begin{pmatrix} 1 & 0 & 0 & 0 \\ 0 & 1 & 0 & 0 \\ -3/(\Delta k_i)^2 & -2/\Delta k_i & 3/(\Delta k_i)^2 & -1/\Delta k_i \\ 1/(\Delta k_i)^3 & 2/(\Delta k_i)^2 & -2/(\Delta k_i)^2 & 1/\Delta k_i \end{pmatrix}$$

$$\left[V(\tau_j) \right]^{-1} = \begin{pmatrix} 1 & 0 & 0 & 0 \\ 0 & 1 & 0 & 0 \\ -3/(\Delta \tau_j)^2 & -2/\Delta \tau_j & 3/(\Delta \tau_j)^2 & -1/\Delta \tau_j \\ 1/(\Delta \tau_j)^3 & 2/(\Delta \tau_j)^2 & -2/(\Delta \tau_j)^2 & 1/\Delta \tau_j \end{pmatrix}$$

Therefore, we can compute the coefficients of the two-dimensional cubic spline, using the following equation:

$$C = \left[V(k_i)\right]^{-1} J \left[V(\tau_j)\right]^{-T} \tag{16}$$

We recognize that there can be an inverse problem in Eq. (16). In fact, the problem comes from selection of the number and location of the grid points, which affect fitting accuracy and smoothness of the two-dimensional cubic spline. When their number and location are optimized, if possible, the approximation power of the two-dimensional cubic spline is improved. However, finding them optimally is a historically difficult problem. To solve this problem, an approach such as estimation of free-knot splines has been proposed (Lindstrom, 1999).

4. NUMERICAL TEST

4.1 Data Description and Screening

We conduct two numerical tests, both of which are based on implied volatility data from market-quoted prices of S&P500 index European option. We acquire our original data sets from Thomson Datastream whose option database contains, on a specific day, the option style (call or put), the, strike price, the trading volume, the option expiration date, the opening, closing, low and high option's price, and the settlement price. We take from this database, for the purpose of our study, the closing call options prices according to strike prices and expiration dates on two specific days. One is May 18th, 2007 and the other June 12th, 2007. The index value is 1522.75 on the first day and 1493.00 on the second day. We assume that we have 252 trading days in a year. The two data sets we choose are screened in order to eliminate the data errors. Firstly, we preclude data where the time to expiry is less than 6 days, since the implied volatility fluctuate very severely even on small error in the corresponding option price (Bakshi *et al*., 1997; Skiadopoulos *et al*., 1999). Secondly, we exclude the entire options that belong to a time to expiry where there are less than 10 strike prices with non-zero contracts traded. Thirdly, we choose data only with the ratio of strike price to spot price ranging from 0.8 to 1.2. Last, we take out from our numerical tests the options with their prices less than their intrinsic values because we know that this is an obvious arbitrage opportunity. After screening our data, we obtain, for 84 strike prices, the option data set consisting of implied volatility and option price quoted by market on the first day. On the second day, we have it for 88 strike prices. Table 1 tells how many strike prices it comprises for each time to maturity in detail on each of the two days.

4.2 Test Results

4.2.1 Result on Data set (I)

To begin with, we construct the implied volatility curve for each time to maturity without the arbitrage-free conditions from Eq. (6) to Eq. (9). In other words, we calibrate the three parameters, a_0, a_1, and a_2, in Eq. (4)

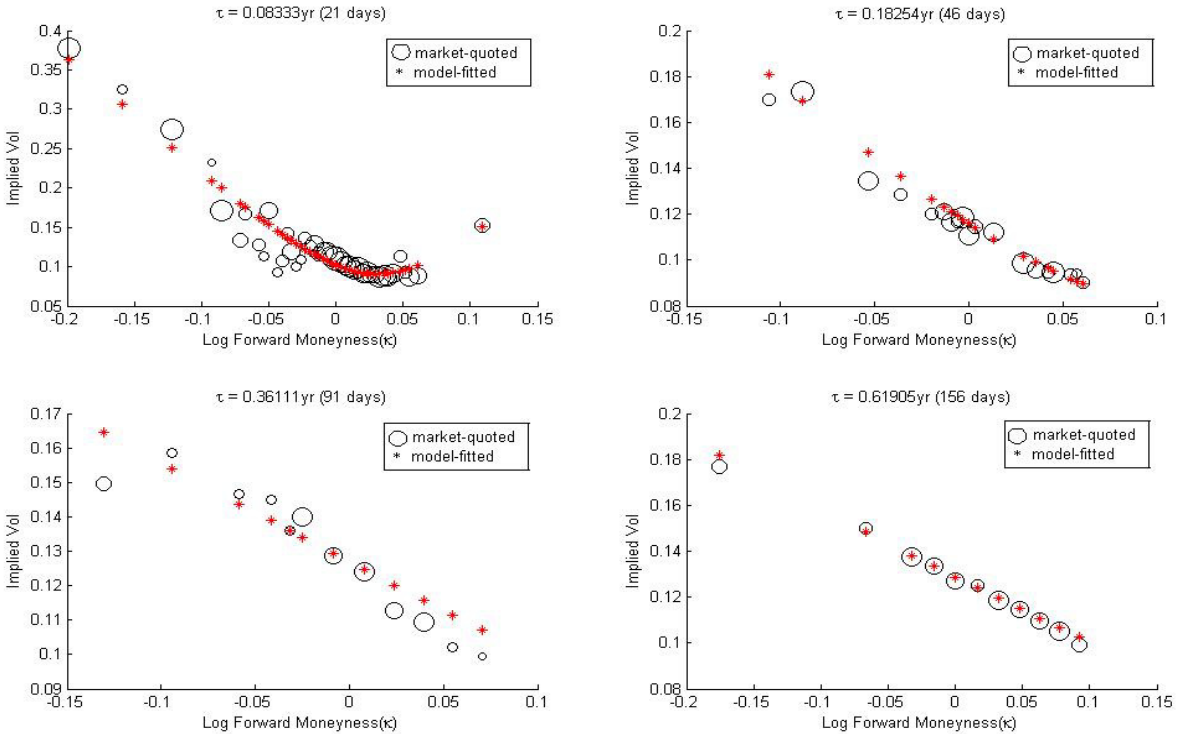

Figure 1. Data Set (I): Market-quoted implied volatilities and Model volatilities fitted from Eq. (4) and Eq. (5)

only with the boundary constraint, Eq. (5). However, the initial parameter setting can influence the calibration. Therefore, after generating 100 initial parameter sets randomly from unit uniform distribution, we conduct it for each of them. Then, we calculate the mean parameter set from the 100 calibrated parameter sets. We put parameter calibration results in Table 2. Figure 1 shows the fitting result computed from the mean parameter set for each of four times to maturity. In the Figure, the red crosses and the black circles mean the implied volatilities fitted from Eq. (4) and Eq. (5) and those quoted in the option market, respectively. Seemingly, our model fits the market data quite well for each time to maturity. However, when we put the four results in Figure 1 together into one figure (Figure 2) in the viewpoint of option price, we can recognize that the results yield an arbitrage. In Figure 2 and Figure 3, the blue color, the red color, the black color, and cyan color indicate the shortest time maturity to the longest maturity in order. The crosses mean the option prices calculated by our model and the circles do the quoted option prices. In particular, let us see Figure 3, which zooms the large black circle in the left upper part of Figure 2. Then, in the in-the-money (small log forward-moneyness) area, our model shows that the option price of the blue circle is larger than that of the red and the black for the same moneyness. This means that our model violates the calendar-spread constraint. Therefore, we need to utilize the constraints referred above.

Next, we build the curves again, including the constraints from Eq. (6) to Eq. (9), producing Figure 4, Figure 5, and Figure 6. In the first two figures, each mark has the same meaning with Figure 1 and Figure 2. Figure 3 also shows that each of the rebuilt curves reflects the quoted implied volatilities well. Moreover, when we see Figure 5 and Figure 6, we cannot observe that the option price of the blue circle is larger than that of the red or that of the black for the same moneyness. Of course, it is also certain that that of the red is smaller than that of the black. In other words, our model with the constraints from Eq. (6) to Eq. (9) constructs the curves free of any arbitrage opportunity. Moreover, we compare our two models in viewpoint of calibration performance. To this end, we make use of two performance measures, which are average MSE (Mean Squared Error) of option price and that of implied volatility. We put calibration performance results in Table 3. As seen in Table 3, our model with the four constraints shows better performance than without them.

Lastly, we construct the implied volatility surface (IVS), using the two-dimensional cubic spline function, Eq. (12), with the grid points as implied volatilities generated from the fitted curves. Figure 7 and Figure 8 show the constructed IVS (black-colored surface) together with the market-quoted implied volatilities (red circles). The first comes from our model with none of the arbitrage-free constraints and the second from our model obtained using them. Both of the surfaces seem to capture well the original quoted implied volatilities. In order to compare the two figures, let us cut them at the

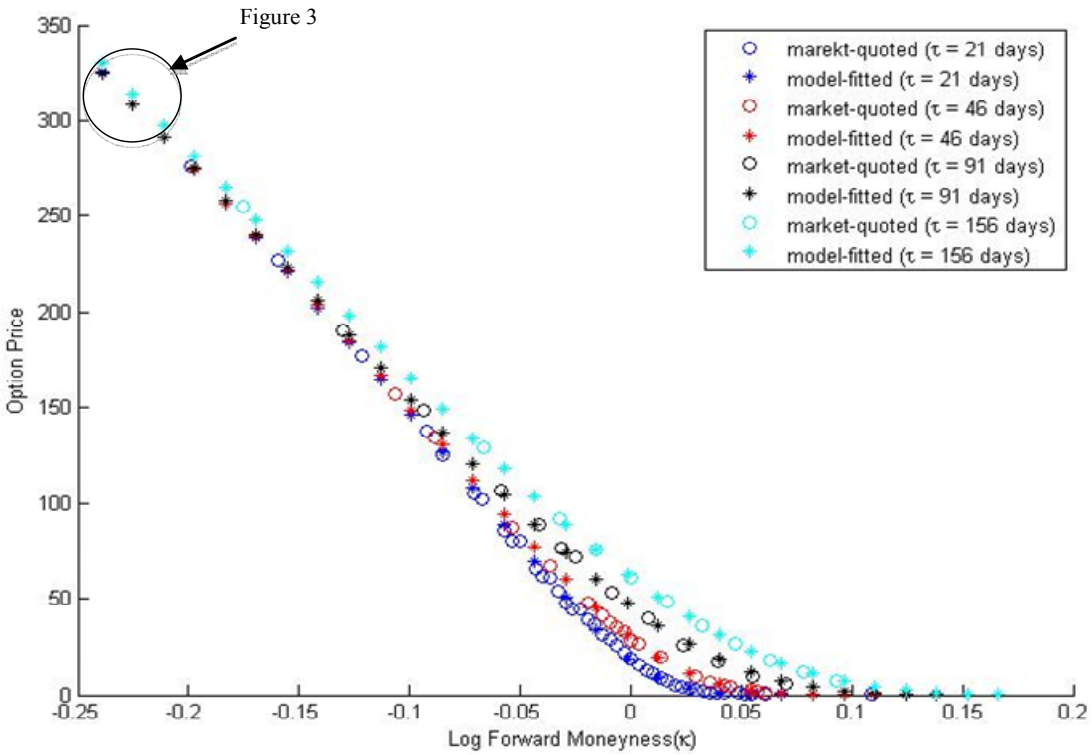

Figure 2. Data Set (I): Comparison of the level of option prices calculated using fitted implied volatilities in Figure 1.

three largest-moneyness values, and then the IVS without them shows more substantial fluctuation with time to maturity than with them. The existing study on implied volatility argues that its smiley or skewed property

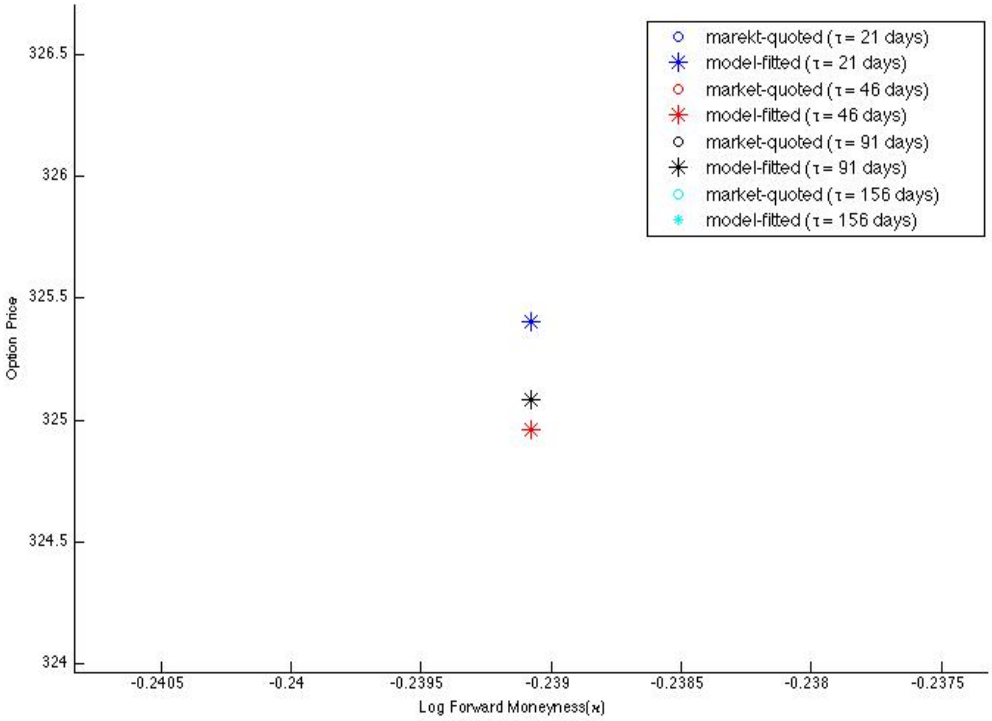

Figure 3. Data Set (I): Arbitrage Opportunity yielded by our model without arbitrage-free constraints.

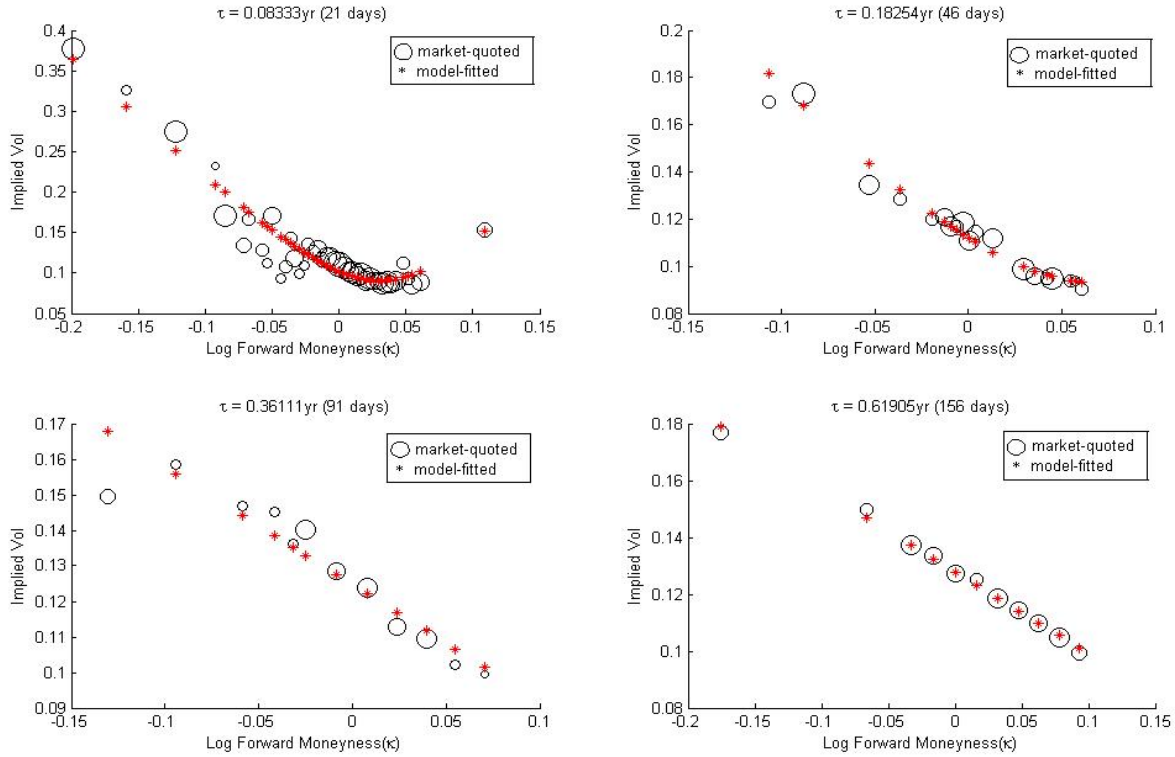

Figure 4. Data Set (I): Market-quoted implied volatilities and Model volatilities fitted from Eq. (4) to Eq. (9).

flattens with time to maturity (Cont and da Fonseca, 2002; Cont and Tankov, 2004). Therefore, the IVS in Figure 8, that is, our model with the constraints shows better calibration.

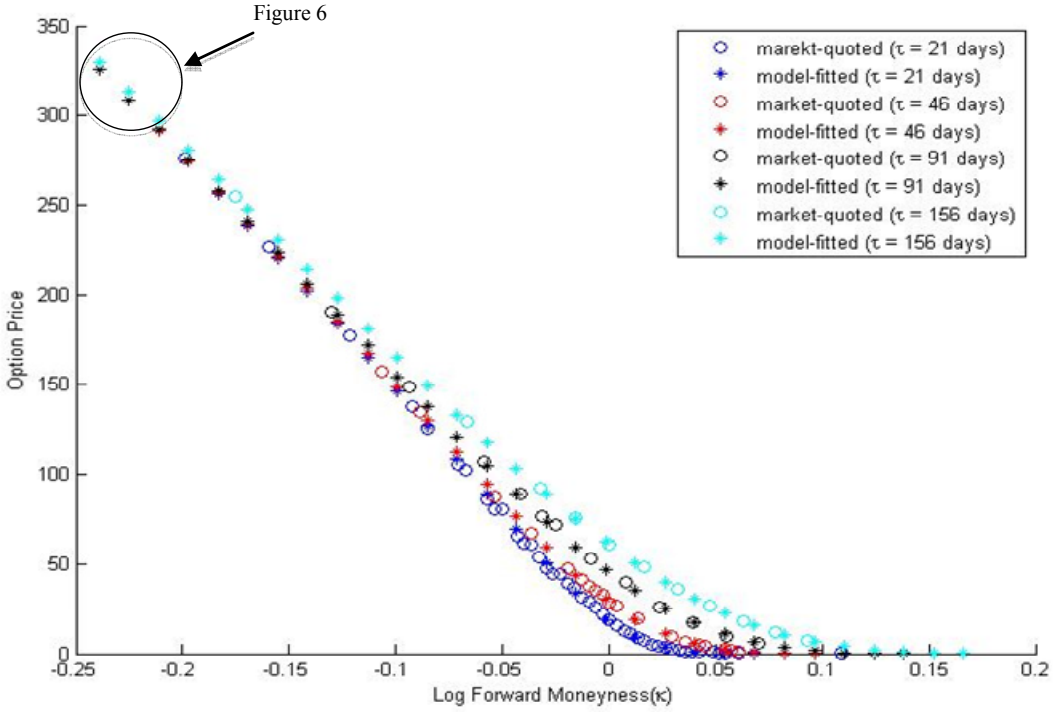

Figure 5. Data Set (I): Comparison of the level of option prices calculated using fitted implied volatilities in Figure 4.

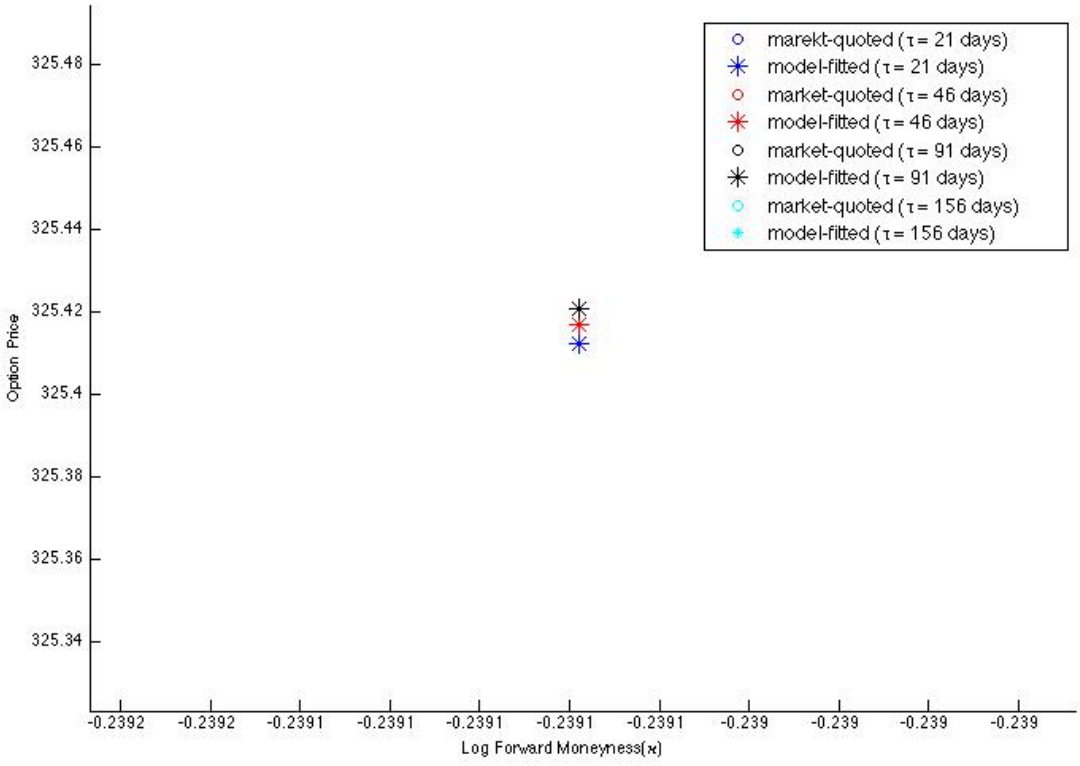

Figure 6. Data Set (I): Arbitrage Opportunity removed by our model with the constraints from Eq. (5) to Eq. (9).

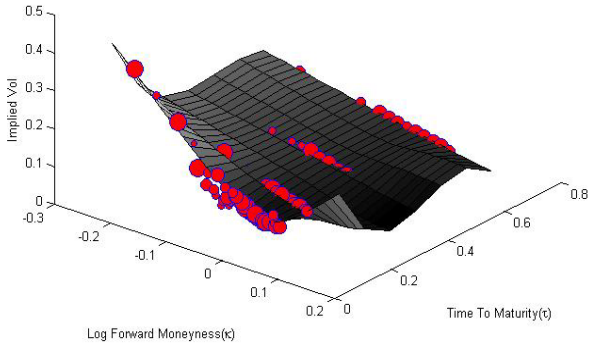

Figure 7. Data Set (I): Implied volatility surface using the curves built from only Eq. (4) and Eq. (5).

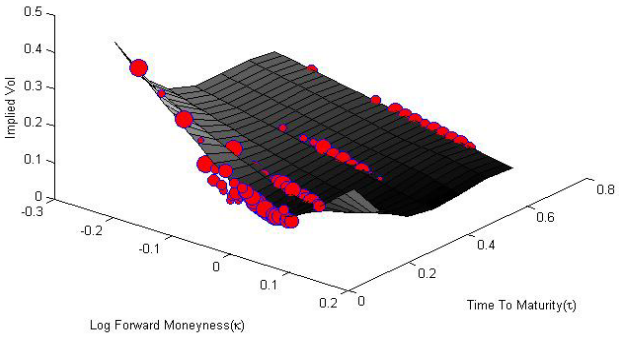

Figure 8. Data Set (I): Implied volatility surface using the curves built from Eq. (4) to Eq. (9).

Table 1. Screened data sets.

Observation Date	Time to maturity (days)	Number of Strike Prices
May 18th - Data Set (I)	21	42
	46	19
	91	12
	156	11
June 12th - Data Set (II)	29	44
	49	12
	74	18
	139	14

4.2.2 Result on Data set (II)

Again, we apply our model to Data set (II). The data set is observed on 12 June 2007 and also includes the implied volatilities related to S&P500 index option like Data set (I) as seen Table 1. We obtain the results corresponding to Section 4.2.1. We see in Figure 10 and Figure 11 that each curve (red crosses) matches with the market-implied volatilities well, and in Figure 12 and Figure 13 that there appears no calendar-spread arbitrage when we compare the four implied volatility curves every forward-moneyness one another. However, like Data Set (I), we have better calibration performance in the model with the arbitrage-free constraints than without them. We also have the calibration results for Data Set (II) in Table 2 and Table 3. We construct the two implied volatility surfaces, Figure 14 and Figure 15, and compare

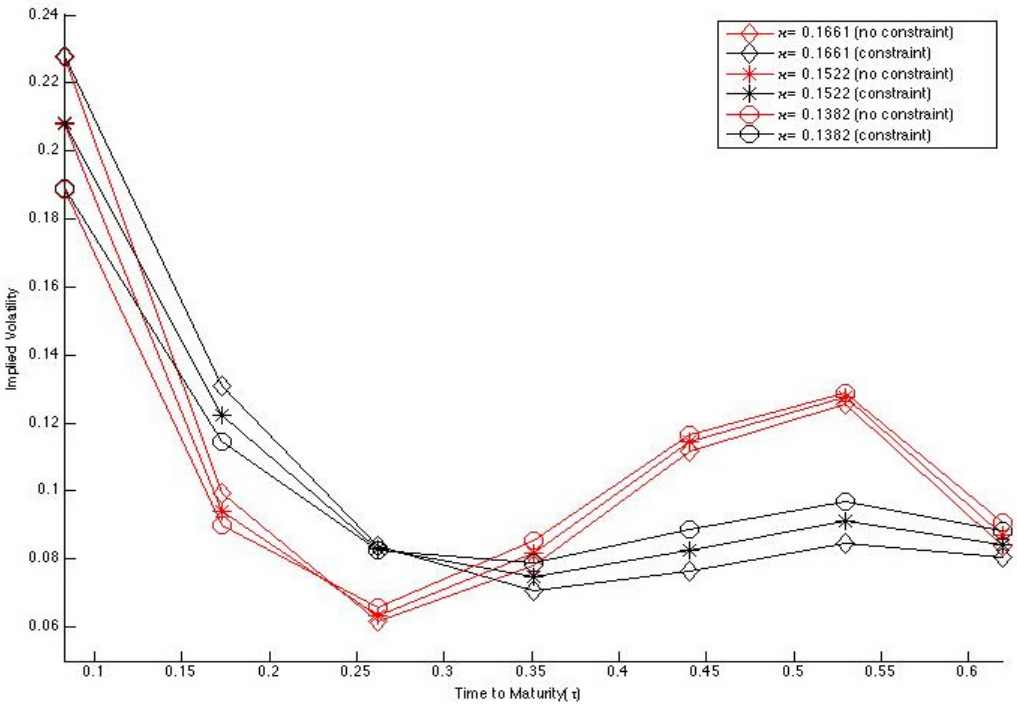

Figure 9. Data Set (I): Implied volatility surfaces cut at log forward-moneyness direction (black lines: use of arbitrage-free constraints, red lines: no use of arbitrage-free constraints).

them, cutting them at log forward-moneyness direction. Let us see Figure 16, and then we can see that the IVS

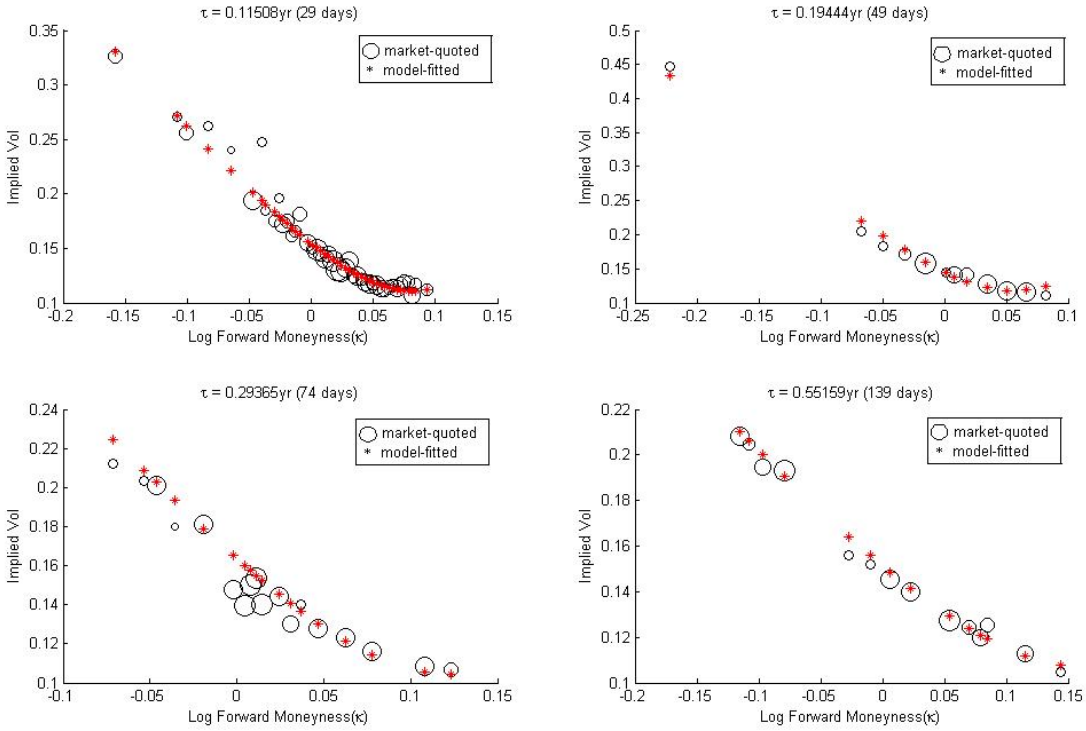

Figure 10. Data Set (II): Market-quoted implied volatilities and Model volatilities fitted from Eq. (4) and Eq. (5).

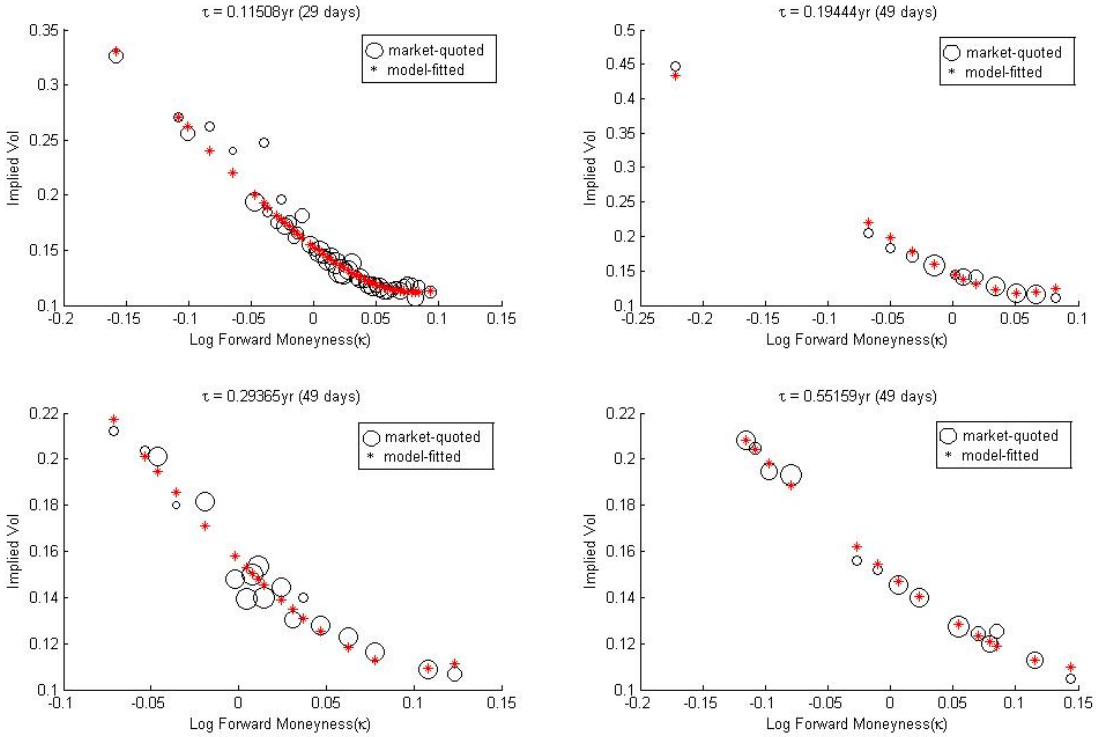

Figure 11. Data Set (II): Market-quoted implied volatilities and Model volatilities fitted from Eq. (4) to Eq. (9).

without the constraints generates negative volatility values and the IVS with them does not. Therefore, we argue that our model with the four arbitrage-free constraints performs better than that without them.

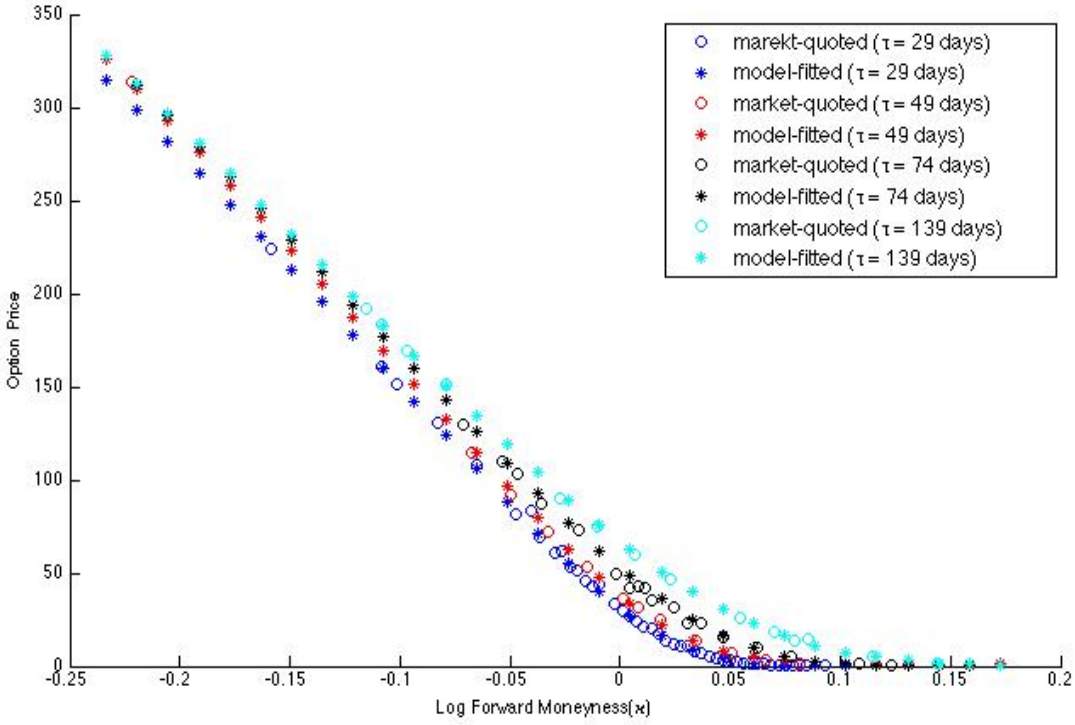

Figure 12. Data Set (II): Comparison of the level of option prices calculated using fitted implied volatilities in Figure 10.

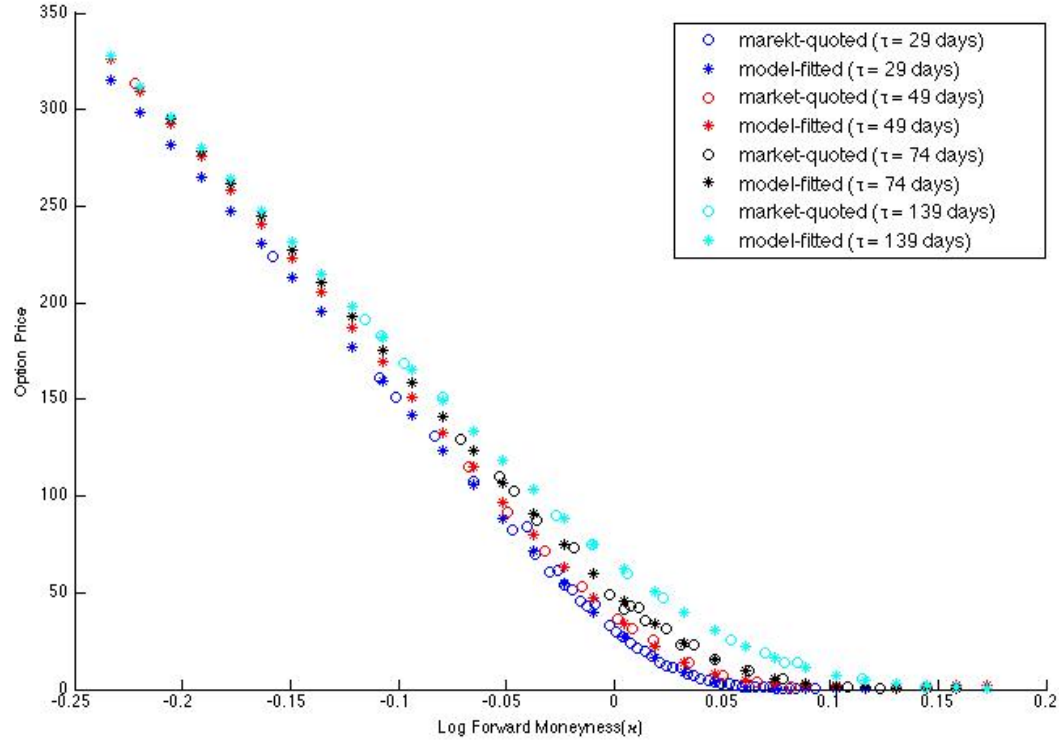

Figure 13. Data Set (II): Comparison of the level of option prices calculated using fitted implied volatilities in Figure 11.

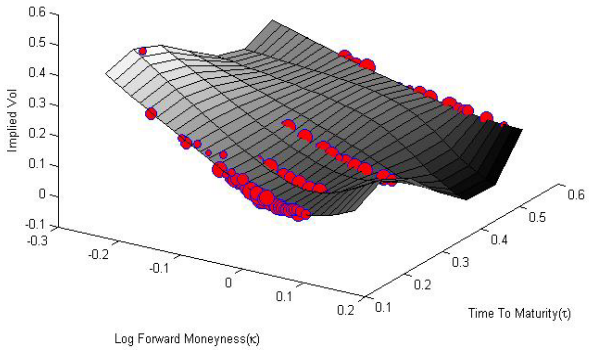

Figure 14. Data Set (II): Implied volatility surface using the curves built from only Eq. (4) and Eq. (5).

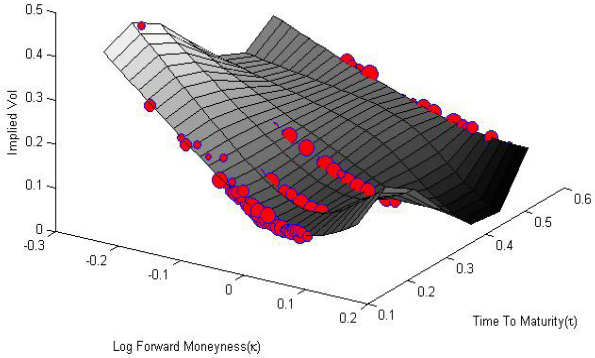

Figure 15. Data Set (II): Implied volatility surface using the curves built from Eq. (4) to Eq. (9).

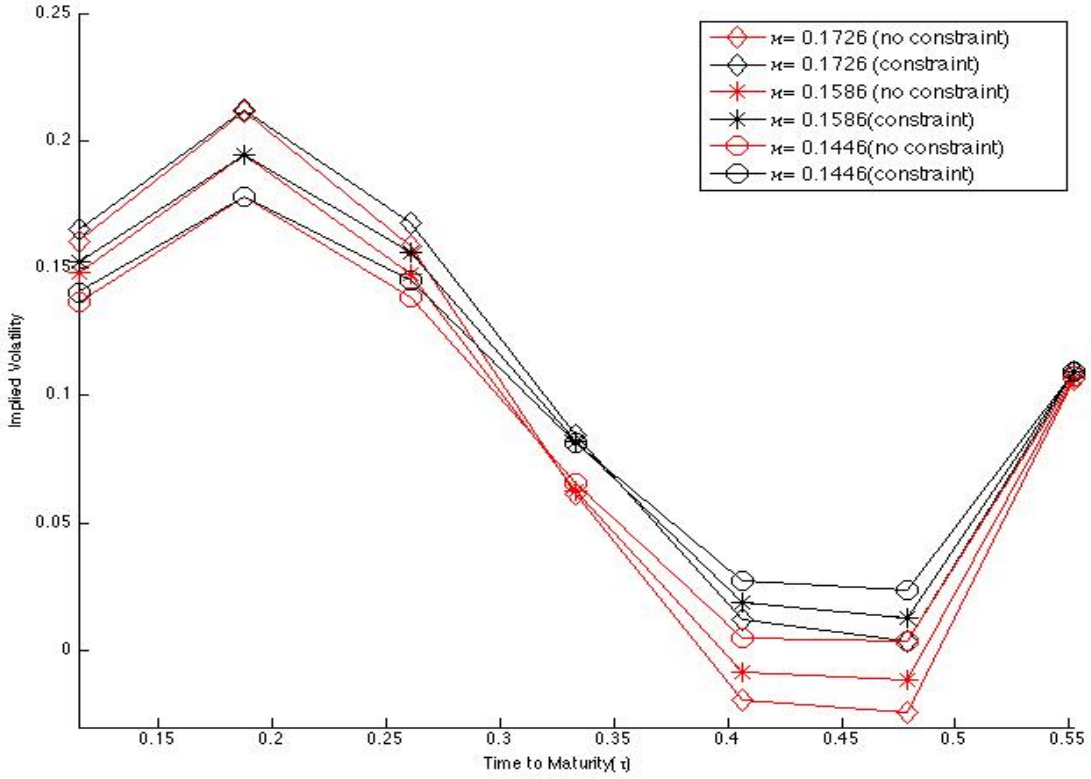

Figure 16. Data Set (II): Implied volatility surfaces cut at log forward-moneyness direction (black lines: use of arbitrage-free constraints, red lines: no use of arbitrage-free constraints).

5. CONCLUSION

In this paper we proposed a model, which builds an IVS using a two-dimensional cubic spline function with its grid points given as implied volatilities computed by optimizing an objective function with the four arbitrage-free conditions from Eq. (6) to Eq. (9). Through all of the optimization processes, we used the interior-point method with the gradients computed from our objective function and nonlinear constraints. To verify the performance of our proposed model, we conducted our simulations with S&P500 European option data we take from Thomson Datastream. In the results of our two data sets, we showed that, before the IVS construction, the implied volatility curves from our proposed model fit well the quoted volatility data without any arbitrage whatever log forward-moneyness or time to maturity in the data sets. Moreover, when establishing the volatility surfaces from the grid points formed by the implied volatility curves, we made sure that the surfaces not only match the original quoted volatility data but also produce no negative volatility. Furthermore, they satisfy the smiley or skewed phenomenon at short maturity and its flattening effect at longer maturity. However, we

need further studies on how to choose grid points automatically and correct the rectangle avoiding negative implied volatility and the fluctuation of IVS. Incorporating kernel-based method in leaves to be further investigated as well (Kim *et al*., 2009; Lee and Lee, 2005; Lee and Lee, 2006; Lee and Lee, 2007; Lee and Lee, 2007; Lee *et al*., 2009).

Table 2. Parameter Calibration Result.

	Mean Calibrated Parameter	**Time to Maturity (Days)**			
May 18th	No Arbitrage Constraint	**21**	**46**	**91**	**156**
	a_0	0.0082	0.0067	0.0021	0.0033
	a_1	2.3654	0.5506	0.0932	0.1058
	a_2	0.0305	0.1111	0.3878	0.3548
	Arbitrage Constraint				
	a_0	0.0082	0.0086	0.0007	0.0005
	a_1	2.3715	0.761	0.1137	0.0862
	a_2	0.0304	0.0724	0.3616	0.4282
June 12th	No Arbitrage Constraint	**29**	**49**	**74**	**139**
	a_0	0.0123	0.0139	0.0109	0.0113
	a_1	1.6732	2.2504	1.0537	0.4048
	a_2	0.0828	0.0566	0.1227	0.1696
	Arbitrage Constraint				
	a_0	0.0126	0.0139	0.012	0.0119
	a_1	1.7082	2.2634	1.145	0.4189
	a_2	0.0798	0.0563	0.1042	0.1584

Table 3. Comparison of Calibration Performance.

	Performance Measure	**No Arbitrage-free Constraint**	**Arbitrage-free Constraint**
May 18th	Average MSE of Option Price	1.7617	1.6111
	Average MSE of Implied Vol.	0.0118	0.0118
June 12th	Average MSE of Option Price	3.0681	2.9234
	Average MSE of Implied Vol.	0.0133	0.0134

ACKNOWLEDGEMENT

This paper was supported by research funds of Chonbuk National University in 2009.

REFERENCES

Andersen, L. B. G. and Brotherton-Ratcliffe, R. (1997), The equity option volatility smile: An implicit finite-difference approach, *Journal of Computational Finance*, **1**(2), 5-37.

Bakshi, G., Cao, C., and Chen, Z. (1997), Empirical Performance of Alternative Option Pricing Models, *Journal of Finance*, **52**, 2003-2049.

Black, F. and Scholes, M. (1973), The Pricing of Options and Corporate Liabilities, *Journal of Politics and Economics*, **81**, 637-654.

Breeden, D. and Litzenberger, R. (1978), Price of state-contingent claims implicit in options prices, *Journal of Business*, **51**, 621-651.

Byrd, R. H., Gilbert, J. C., and Nocedal, J. (2000), A Trust Region Method Based on Interior Point Techniques for Nonlinear Programming, *Mathematical Programming*, **89**, 149-185.

Byrd, R. H., Hribar, M. E., and Nocedal, J. (1999), An Interior Point Algorithm for Large-Scale Nonlinear Programming, *SIAM Journal on Optimization*, **9**, 877-900.

Carr, P. and Madan, D. B. (2005), A Note on Sufficient Conditions for No Arbitrage, *Finance Research Letters*, **2**, 125-130.

Cont, R. and da Fonseca, J. (2002), Dynamics of Implied Volatility Surfaces, *Quantitative Finance*, **2**, 45-60.

Cont, R. and Tankov, P. (2004), Financial Modeling with Jump Processes, Chapman and Hall, Florida.

de Boor, C. (1962), Bicubic Spline Interpolation, *Journal of Mathematical Physics*, **41**, 212-218.

Dempster, M. A. H. and Richards, D. G. (2000), Pricing American options fitting the smile, *Mathematical Finance*, **10**(2), 157-177.

Derman, E. and Kani, I. (1994), Riding on a smile, *RISK*, **7**(2), 32-39.

Dumas, B., Fleming, J., and Whaley, R. E. (1998), Implied Volatility Functions: Empirical Tests, *Journal of Finance*, **53**, 2059-2106.

Dupire, B. (1994), Pricing with a Smile, *RISK*, **7**(1), 18-20.

Konstantinidi, E., Skiadopoulos, G., and Tzagkaraki, E. (2008), Can the Evolution of Implied Volatility be Forecasted? Evidence from European and US Implied Volatility Indices, *Journal of Banking and Finance*, **32**, 2401-2411.

Fengler, M. R. (2005), Arbitrage-free Smoothing of the Implied Volatility Surface, *Quantitative Finance*, **9**, 417-428.

Han, G.-S. and Lee, J. (2008), Prediction of pricing and hedging errors for equity linked warrants with Gaussian process models, *Expert Systems with Applications*, **35**, 515-523.

Han, G.-S., Kim, B.-H., and Lee, J. (2009), Kernel-based Monte Carlo simulation for American option pricing, *Expert Systems with Applications*, **36**, 4431-4436.

Hull, J. H. (2009), Option, Futures, and Other Derivatives 7th edition, Prentice Hall, New Jersey.

Kim, N.-H., Lee, J., and Han, G.-S. (2009), Model Averaging Methods for Estimating Implied Volatility and Local Volatility Surfaces, *Industrial Engineering and Management Science*, **8**(2), 93-100.

Lee, J. and Lee, D.-W. (2005), An Improved Cluster Labeling Method for Support Vector Clustering, *IEEE Trans. on Pattern Analysis and Machine Intelligence*, **27**, 461-464.

Lee, J. and Lee, D.-W. (2006), Dynamic Characterization of Cluster Structures for Robust and Inductive Support Vector Clustering, *IEEE Trans. on Pattern Analysis and Machine Intelligence*, **28**, 1869-1874.

Lee, D.-W. and Lee, J. (2007), Domain Described Support Vector Classifier for Multi-Classification Problems, *Pattern Recognition*, **40**, 41-51.

Lee, D.-W. and Lee, J. (2007), Equilibrium-Based Support Vector Machine for Semi-Supervised Classification, *IEEE Trans. on Neural Networks*, **18**, 578-583.

Lee, D.-W., Jung, K.-H., and Lee, J. (2009), Constructing Sparse Kernel Machines Using Attractors, *IEEE Trans. on Neural Networks*, **20**, 721-729.

Lindstrom, M. J. (1999), Penalized Estimation of Free-Knot Splines, *Journal of Computational and Graphical Statistics*, **8**, 333-352.

Parkinson, M. (1980), The Extreme Value Method for Estimating the Variance of the Rate of Return, *Journal of Business*, **53**, 61-68.

Rogers, L. and Satchell. S. (1991), Estimating Variance from High, Low and Closing Prices, *Annals of Applied Probability,* **1**, 504-512.

Rogers, L., Satchell, S., and Yoon, Y. (1994), Estimating the Volatility of Stock Prices: A Comparison of Methods that Use High and Low Prices, *Applied Financial Economics*, **4**, 241-247.

Rubinstein, M. (1994), Implied Binomial Trees, *Journal of Finance,* **49**, 771-818.

Späth, H. (1995), Two Dimensional Spline Interpolation Algorithms, A K Peters, Boston.

Skiadopoulos G., Hodges, S., and Clewlow, L. (1999), The Dynamics of the S&P 500 Implied Volatility Surface, *Review of Derivatives Research*, **3**, 263-282.

Waltz, R. A., Morales, J. L., Nocedal, J., and Orban, D. (2006), An Interior Algorithm for Nonlinear Optimization that Combines Line Search and Trust Region Steps, *Mathematical Programming*, **107**, 391-408.

APPENDIX

1. Proof of Proposition

If, in order to calculate an European call option, we set its present underlying asset value, strike price, time to maturity, and probability density function as S_0, K, τ, and φ, respectively, the call option value (V) can be expressed as

$$V(S_0, K, \tau) = Call(S_0, K, \tau) = e^{-r\tau}\int_0^{+\infty} \max(S_\tau - K, 0)\varphi(S_\tau, \tau | S_0, 0)dS_\tau$$

Then,

$$\begin{aligned} e^{r\tau}V(S_0, K, \tau) &= \int_0^{+\infty} \max(S_\tau - K, 0)\varphi(S_\tau, \tau | S_0, 0)dS_\tau \\ &= \int_K^{+\infty} S_\tau\varphi(S_\tau, \tau | S_0, 0)dS_\tau - K\int_K^{+\infty} \varphi(S_\tau, \tau | S_0, 0)dS_\tau \\ e^{r\tau}\frac{\partial V}{\partial K} &= -K\varphi(K, \tau | S_0, 0) \\ &\quad -\int_K^{+\infty} \varphi(S_\tau, \tau | S_0, 0)dS_\tau + K\varphi(K, \tau | S_0, 0) \\ &= -\int_K^{+\infty} \varphi(S_\tau, \tau | S_0, 0)dS_\tau \\ &= \int_{-\infty}^{K} \varphi(S_\tau, \tau | S_0, 0)dS_\tau - 1 = \Phi(K, \tau | S_0, 0) - 1 \quad \text{(A1)} \end{aligned}$$

Moreover, using the forward price of underlying asset, F_0, we can also represent the option value as

$$V = e^{-r\tau}\{F_0 N(d_1) - KN(d_2)\}$$

Therefore,

$$e^{r\tau}\frac{\partial V}{\partial K} = -N(d_2) + F_0\dot{d}_1 n(d_1) - K\dot{d}_2 n(d_2)$$

Inserting this result into the result noted by Eq. (A-1), we obtain

$$\Phi(k, \tau | F_0) = 1 - N(d_2) + F_0\dot{d}_1 n(d_1) - K\dot{d}_2 n(d_2)$$

Then, the remaining results can be attained obviously with simple derivative calculations. □

2. Interior-point Algorithm with CG (Conjugate Gradient)

The interior-point approach to constrained minimization is to solve a sequence of approximate minimization problems.

The original problem is

$$\min_x f(x), \text{ subject to } h(x) = 0 \text{ and } g(x) \le 0 \quad \text{(A-2)}$$

For each $\mu > 0$, we can approximate the problem (A-2) in the following way:

$$\begin{aligned} &\min_{x,\mu} f_\mu(x, s) = \min_{x,s} f(x) - \mu\sum_i \ln(s_i) \\ &\text{subject to } h(x) = 0,\ g(x) + s = 0, \text{ and } s > 0 \quad \text{(A-3)} \end{aligned}$$

The number of dimension of the inequality constraint $g(x)$ is the same with that of the slack variable s. As μ approaches to zero, the minimum of f_μ should go toward the minimum of f. The added logarithmic term is called a barrier function. This algorithm is explained in Byrd *et al*., 2000; Byrd *et al*., 1999, and Waltz *et al*., 2006. The approximate problem (A-3) is transformed into a sequence of equality-constrained problems. One of the solutions to (A-3) is to use the conjugate gradient approach. In this case, we adjust both x and s, keeping s positive. The approach is to minimize a quadratic approximation to the problem (A-3) in a trust region, subject to linearized constraints. Specifically, let R denote the radius of the trust region, then we acquire Lagrange multipliers (λ and y) by approximately solving the KKT equations:

$$\nabla_x L = \nabla_x f(x) + \sum_i \lambda_i \nabla g_i(x) + \sum_j y_i \nabla h_j(x) = 0 \qquad \text{(A-4)}$$

in the least-squares sense, subject to λ being positive. Then we take a step (Δx, Δs) to approximately solve

$$\min_{\Delta x, \Delta s} \nabla f^T \Delta x + \frac{1}{2}\Delta x^T \nabla_{xx}^2 L \Delta x + \mu 1^T S^{-1}\Delta s + \frac{1}{2}\Delta s^T S^{-1}\Lambda \Delta s \quad \text{(A-5)}$$

subject to the linearized constraints

$$g(x) + J_g \Delta x + \Delta s = 0, \;\; h(x) + J_h \Delta x = 0 \qquad \text{(A-6)}$$

In Eq. (A-5) and Eq. (A-6), 1 is a vector of ones the same size with $g(x)$, S and Λ are diagonal matrices with s and λ, respectively, and J_g and J_h are the Jacobian of the constraint $g(x)$ and $h(x)$, respectively. Then, in order to solve Eq. (A-6), we try to minimize a norm of the linearized constraints inside a region with radius scaled by R. Eq. (A-5) is solved with the constraints being to match the residual from solving Eq. (A-6), staying within the trust region of radius R, and keeping s strictly positive.

3. Connection Matrix J

$$J = \begin{pmatrix} u_{ij} & q_{ij} & u_{i,j+1} & q_{i,j+1} \\ p_{ij} & r_{ij} & p_{i,j+1} & r_{i,j+1} \\ u_{i+1,j} & q_{i+1,j} & u_{i+1,j+1} & q_{i+1,j+1} \\ p_{i+1,j} & r_{i+1,j} & p_{i+1,j+1} & r_{i+1,j+1} \end{pmatrix}$$

Each element of the above matrix J is calculated as follows:

$$u_{ij} = \Sigma_{ij}(k_i, \tau_j) = \begin{pmatrix} 1 & 0 & 0 & 0 \end{pmatrix} C \begin{pmatrix} 1 \\ 0 \\ 0 \\ 0 \end{pmatrix}$$

$$u_{i,j+1} = \Sigma_{ij}(k_i, \tau_{j+1}) = \begin{pmatrix} 1 & 0 & 0 & 0 \end{pmatrix} C \begin{pmatrix} 1 \\ \Delta\tau_j \\ (\Delta\tau_j)^2 \\ (\Delta\tau_j)^3 \end{pmatrix}$$

$$u_{i+1,j} = \Sigma_{ij}(k_{i+1}, \tau_j) = \begin{pmatrix} 1 & \Delta k_i & (\Delta k_i)^2 & (\Delta k_i)^3 \end{pmatrix} C \begin{pmatrix} 1 \\ 0 \\ 0 \\ 0 \end{pmatrix}$$

$$u_{i+1,j+1} = \Sigma_{ij}(k_{i+1}, \tau_{j+1}) = \begin{pmatrix} 1 & \Delta k_i & (\Delta k_i)^2 & (\Delta k_i)^3 \end{pmatrix} C \begin{pmatrix} 1 \\ \Delta\tau_j \\ (\Delta\tau_j)^2 \\ (\Delta\tau_j)^3 \end{pmatrix}$$

$$p_{ij} = \left.\frac{\partial \Sigma_{ij}}{\partial k}\right|_{k=k_i, \tau=\tau_j} = \begin{pmatrix} 0 & 1 & 0 & 0 \end{pmatrix} C \begin{pmatrix} 1 \\ 0 \\ 0 \\ 0 \end{pmatrix}$$

$$p_{i,j+1} = \left.\frac{\partial \Sigma_{ij}}{\partial k}\right|_{k=k_i, \tau=\tau_{j+1}} = \begin{pmatrix} 0 & 1 & 0 & 0 \end{pmatrix} C \begin{pmatrix} 1 \\ \Delta\tau_j \\ (\Delta\tau_j)^2 \\ (\Delta\tau_j)^3 \end{pmatrix}$$

$$p_{i+1,j} = \left.\frac{\partial \Sigma_{ij}}{\partial k}\right|_{k=k_{i+1}, \tau=\tau_j} = \begin{pmatrix} 0 & 1 & 2\Delta k_i & 3(\Delta k_i)^2 \end{pmatrix} C \begin{pmatrix} 1 \\ 0 \\ 0 \\ 0 \end{pmatrix}$$

$$p_{i+1,j+1} = \left.\frac{\partial \Sigma_{ij}}{\partial k}\right|_{k=k_{i+1}, \tau=\tau_{j+1}} = \begin{pmatrix} 0 & 1 & 2\Delta k_i & 3(\Delta k_i)^2 \end{pmatrix} C \begin{pmatrix} 1 \\ \Delta\tau_j \\ (\Delta\tau_j)^2 \\ (\Delta\tau_j)^3 \end{pmatrix}$$

$$q_{ij} = \left.\frac{\partial \Sigma_{ij}}{\partial \tau}\right|_{k=k_i, \tau=\tau_j} = \begin{pmatrix} 1 & 0 & 0 & 0 \end{pmatrix} C \begin{pmatrix} 0 \\ 1 \\ 0 \\ 0 \end{pmatrix}$$

$$q_{i,j+1} = \left.\frac{\partial \Sigma_{ij}}{\partial \tau}\right|_{k=k_i, \tau=\tau_{j+1}} = \begin{pmatrix} 1 & 0 & 0 & 0 \end{pmatrix} C \begin{pmatrix} 0 \\ 1 \\ 2\Delta\tau_j \\ 3(\Delta\tau_j)^2 \end{pmatrix}$$

$$q_{i+1,j} = \left.\frac{\partial \Sigma_{ij}}{\partial \tau}\right|_{k=k_{i+1}, \tau=\tau_j} = \begin{pmatrix} 1 & \Delta k_i & (\Delta k_i)^2 & (\Delta k_i)^3 \end{pmatrix} C \begin{pmatrix} 0 \\ 1 \\ 0 \\ 0 \end{pmatrix}$$

$$q_{i+1,j+1} = \left.\frac{\partial \Sigma_{ij}}{\partial \tau}\right|_{k=k_{i+1}, \tau=\tau_{j+1}} = \begin{pmatrix} 1 & \Delta k_i & (\Delta k_i)^2 & (\Delta k_i)^3 \end{pmatrix} C \begin{pmatrix} 0 \\ 1 \\ 2\Delta\tau_j \\ 3(\Delta\tau_j)^2 \end{pmatrix}$$

$$r_{ij}=\left.\frac{\partial^2\Sigma_{ij}}{\partial k\partial\tau}\right|_{k=k_i,\tau=\tau_j}=\begin{pmatrix}0 & 1 & 0 & 0\end{pmatrix}C\begin{pmatrix}0\\1\\0\\0\end{pmatrix}$$

$$r_{i+1,j}=\left.\frac{\partial^2\Sigma_{ij}}{\partial k\partial\tau}\right|_{k=k_{i+1},\tau=\tau_j}=\begin{pmatrix}0 & 1 & 2\Delta k_i & 3\left(\Delta k_i\right)^2\end{pmatrix}C\begin{pmatrix}0\\1\\0\\0\end{pmatrix}$$

$$r_{i,j+1}=\left.\frac{\partial^2\Sigma_{ij}}{\partial k\partial\tau}\right|_{k=k_i,\tau=\tau_{j+1}}=\begin{pmatrix}0 & 1 & 0 & 0\end{pmatrix}C\begin{pmatrix}0\\1\\2\Delta\tau_j\\3\left(\Delta\tau_j\right)^2\end{pmatrix}$$

$$r_{i+1,j+1}=\left.\frac{\partial^2\Sigma_{ij}}{\partial k\partial\tau}\right|_{k=k_{i+1},\tau=\tau_{j+1}}=\begin{pmatrix}0 & 1 & 2\Delta k_i & 3\left(\Delta k_i\right)^2\end{pmatrix}C\begin{pmatrix}0\\1\\2\Delta\tau_j\\3\left(\Delta\tau_j\right)^2\end{pmatrix}$$